Chasing snails

Duller, G. A.T.; Roberts, H. M.

Published in:
Radiation Measurements

DOI:
10.1016/j.radmeas.2024.107084

Publication date:
2024

Citation for published version (APA):
Duller, G. A. T., & Roberts, H. M. (2024). Chasing snails: Automating the processing of EMCCD images of luminescence from opercula. *Radiation Measurements*, *172*, Article 107084. https://doi.org/10.1016/j.radmeas.2024.107084

Radiation Measurements 172 (2024) 107084

Contents lists available at ScienceDirect

Radiation Measurements

journal homepage: www.elsevier.com/locate/radmeas

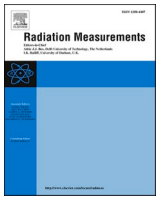

Chasing snails: Automating the processing of EMCCD images of luminescence from opercula

G.A.T. Duller *, H.M. Roberts

Department of Geography and Earth Sciences, Aberystwyth University, Aberystwyth, Ceredigion, SY23 3DB, UK

ARTICLE INFO

Keywords:
Imaging
Luminescence
EMCCD
Data analysis
Calcite
TL

ABSTRACT

Opercula of the gastropod *Bithynia tentaculata* are composed of calcite, and are typically 2–4 mm in length. They emit a thermoluminescence (TL) signal that can be used for dose reconstruction, and spatially resolved TL data from them can be obtained using an electron multiplying charge coupled device (EMCCD). However, when multiple measurements are made of the same sample with imaging detectors such as the EMCCD, registering the different images is crucial so that when regions of interest (ROI) are defined they consistently relate to the same part of the specimen. Previous work on opercula has undertaken this registration by hand, but this is prohibitively time consuming and is also potentially prone to human error. An automated registration process is described, and its use is illustrated using a dose recovery experiment. Without registration more than half of the regions of interest defined across the operculum failed the recycling test, and for those ROIs which did pass recycling the dose recovery ratio varied from 0.7 to 1.2. After registration more than 97% of ROIs passed recycling and all these ROIs gave dose recovery ratios within two sigma of unity. The automated registration process described here has potential for application to other types of solid sample such as rock slices provided they are not perfectly circular.

1. Introduction

The majority of luminescence measurements for dose reconstruction or geological and archaeological dating use photomultiplier tubes (PMTs) to detect the emitted light. Such devices detect emissions from anywhere across the sample, and do not normally provide any information about which part of the sample is emitting luminescence. Spatially resolved optically stimulated luminescence measurements are possible with a PMT by scanning with the stimulation source (e.g. Bailiff and Mikhailik 2003; Sanderson et al., 2001; Duller et al., 1999), but such an approach is much more challenging for thermoluminescence (TL) measurements. Spatially resolved TL requires some type of imaging device. Devices for imaging luminescence emissions based around sensitive photographic films or image intensifiers have been used for a number of years (e.g. Walton and Debenham 1980; Hashimoto et al., 1983; Smith et al., 1991).

The advent of charge coupled devices (CCDs) transformed digital imaging, and although early devices had limited sensitivity they were utilised in a number of luminescence applications (e.g. Duller et al., 1997; Greilich et al., 2002; Baril 2004). Rapid improvements in digital imaging occurred, including the development of electron multiplying charge coupled devices (EMCCD) where the read noise that is a common impediment when using CCDs is overcome by multiplying the charge as it is clocked out of the sensor and prior to digitisation (McWhirter, 2008). A number of experimental instruments have been developed using such detectors (e.g. Clark-Balzan and Schwenninger, 2012), and in more recent years they have been integrated into commercially available luminescence instruments (e.g. Richter et al., 2013; Kook et al., 2015).

However, where analysis of a sequence of measurements of the luminescence signal following different treatments is required, a challenge facing all imaging systems has been to accurately register the images so that a signal measured from a region of interest defined in one image is compared with the light emitted from the corresponding part of the other images in the sequence of measurements (Duller et al., 1997). This is true of all types of imaging (e.g. Sellwood et al., 2022), but is particularly an issue with automated instruments where sample repositioning varies from one measurement step to the next, resulting in samples potentially moving laterally and rotationally with respect to the field of view of the imaging device. Kook et al. (2015) were able to

* Corresponding author.
E-mail address: ggd@aber.ac.uk (G.A.T. Duller).

https://doi.org/10.1016/j.radmeas.2024.107084
Received 15 November 2023; Received in revised form 15 February 2024; Accepted 26 February 2024
Available online 27 February 2024

automate this registration process for measurements of the OSL signal from single grains by mounting grains within a specially designed holder (Bøtter-Jensen et al., 2000) where the grains are spaced regularly and their location can be determined using fixed locating holes. For other types of samples mounted on the surface of a disc or cup and free to move during measurement, registration remains a major challenge.

The calcitic opercula of *Bithynia tentaculata* are of interest for their TL emission which grows to doses in excess of 8000 Gy (Duller and Roberts, 2018), meaning it is potentially able to date the entire Quaternary period. The opercula are teardrop shaped and typically 2–4 mm on their longest axis. Imaging using an EMCCD permits spatially resolved equivalent dose determination using the TL signal, but registering the images has been a major impediment to analysis of sequences of measurements. Previous work by Duller et al. (2015) manually determined the translation and rotation of the opercula using distinctive features on the periphery of the opercula as markers. However, this approach is time consuming, especially where between 30 and 50 images of each operculum may need to be aligned for a single sequence of measurements, and the approach is also prone to human error.

The aim of this paper is to describe the development of an automated process of image registration capable of tracking each operculum, dramatically reducing data processing time. The ImageJ suite of imaging tools is used for some of the processing (Schneider et al., 2012), implemented in FIJI, and the results integrated into existing analytical tools for luminescence palaeodosimetry to allow equivalent dose (D_e) determination.

2. Equipment and samples

All measurements were made on a Risø TL/OSL reader DA-20 equipped with an Evolve-512 EMCCD running at −80 °C. Focussing within the control software was optimised for a wavelength of 550 nm (the primary emission from opercula, Duller et al., 2009), with a height setting of 0.9 mm, and opening the aperture to 21.9 mm for TL measurements to maximise the collection of light. The 512 by 512 pixel sensor yields an effective resolution of 19 μm per pixel. All thermoluminescence images were collected through a 2 mm thick Schott BG-39 filter, and after every measurement of luminescence the same EMCCD was used to collect a reflected light image illuminated with the IR LEDs (870 nm) operated at 0.1% of full power. The image was collected with no optical filter, and with the aperture for the camera reduced to the lowest setting of 2.2 mm in order to sharpen the image. This visible image records the position of the operculum, and can be used to determine any lateral or rotational movement between measurements. Opercula of the gastropod *Bithynia tentaculata* were picked by hand from sediment samples, cleaned in an ultrasonic bath to remove adhering sediment grains, and then placed on steel cups for TL measurement.

The data processing methods developed here are applicable to any set of measurements, but are illustrated using a single aliquot regenerative dose (SAR) protocol developed for TL measurements of calcitic opercula (Table 1). A typical SAR sequence for opercula generates six EMCCD data sets per cycle, meaning that measuring the natural signal and eight regeneration doses (including one or two zero dose points) will produce 54 visible images for each operculum. The volume of data and the need to register data reproducibly are the drivers for developing an automated approach.

Table 1
Single aliquot regenerative dose (SAR) protocol used for D_e determination of opercula.

Step		Purpose
1	Regeneration Dose	
2	TL to 320 °C at 0.5 °C.s^{-1}	Preheat
3	TL to 400 °C at 0.5 °C.s^{-1}	L_x (signal)
4	TL to 400 °C at 0.5 °C.s^{-1}	L_x (blackbody)
5	Test Dose	
6	TL to 320 °C at 0.5 °C.s^{-1}	Preheat
7	TL to 400 °C at 0.5 °C.s^{-1}	T_x (signal)
8	TL to 400 °C at 0.5 °C.s^{-1}	T_x (blackbody)

Note: During all TL measurements one data point (one frame) was collected per degree centigrade (i.e. one frame every 2 s).

3. Automated identification of opercula, and assessing their movement

The first objective in processing the visible images collected from the Risø system is to isolate the operculum from the remainder of the image. The initial 16-bit image (Fig. 1a) has the brightness and contrast stretched (Fig. 1b), and a threshold is applied to convert the image to a binary image, attempting to differentiate between the object of interest (the operculum) and the rest of the image (the background) (Fig. 1c). Whilst selecting a threshold value manually is possible, it is time consuming and is generally not reproducible. A range of different automated thresholding methods have been reviewed by Sezgin and Sankur (2004), and many are implemented in ImageJ. The optimal thresholding method for the current application appears to be that of Li (described in Sezgin and Sankur, 2004) based on analysis of the entropy of the image and the resulting binary image.

As well as picking out the operculum, the thresholding method also normally picks out the edges of the steel cup where the infrared light is reflected into the detector (Fig. 1c). To select only the operculum, differences in the size and circularity of the cup edges compared with the operculum are used. The final part of this initial identification of the operculum applies a particle analyser function, set to only identify objects whose circularity is above a value of 0.10 and whose area is above 15,000 pixels (5.4 mm^2). The resulting image only shows the operculum (Fig. 1d) and from this image it is possible to determine the two-dimensional morphology of the operculum, including the area, the maximum length (the a-axis) and the width (b-axis).

Thresholding the image is a critical step in this process, and provides an assessment of where the edge of the operculum is on each image. The majority of opercula have very distinct edges, though in some cases it is seen that the edges can be almost translucent, making it hard for the thresholding to accurately define the edge. To assess how reproducibly the thresholding is able to identify opercula, the morphological parameters can be calculated for each image within a sequence. A typical example is shown in Fig. 2. The movement of the operculum laterally and rotationally can be seen during 54 measurements (Fig. 2a). The area calculated for each of the 54 visible images is shown in Fig. 2b, and for this example this yields an average area of 40,078 pixels (14.5 mm^2), with a standard deviation of only 31 pixels (relative standard deviation (RSD) of 0.08%). The a-axis of the operculum is also calculated for each image, and this yields a value of 278.1 ± 0.5 pixels (RSD 0.19 %), equivalent to 5.3 mm.

Where analysis of a set of images from an operculum does not yield consistent estimates of the area of the operculum this is a result of the thresholding method not consistently isolating the operculum and may result from subtle changes in lighting as the sample rotates. Such failures are unusual, but where they occur they can normally be resolved by picking an alternative thresholding method, either based on entropy like Li (methods such as those by Renyi or the Maximum entropy method), or based on attribute identification (such as the Huang method).

4. Registering images

The opercula being studied do not deform during measurement and so they can be treated as a rigid-body. To register the multiple images collected during a sequence requires calculation of the lateral movement of the object and any rotation. Such information could be derived from the a-axis positions shown in Fig. 2a, but since this only measures the maximum dimension of the operculum it is prone to errors. A more robust approach is to determine the movement of the whole object by

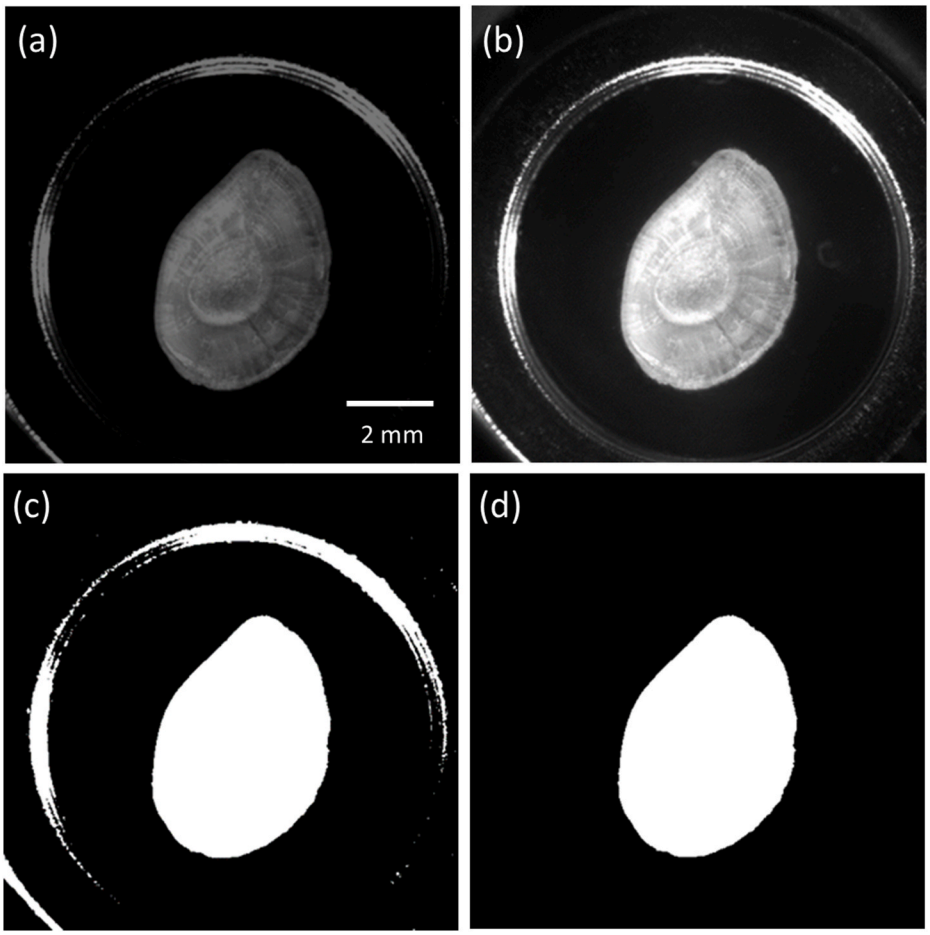

Fig. 1. Initial processing of visible images to identify an operculum. The raw image (a) collected from the EMCCD has its brightness and contrast enhanced to produce image (b). A thresholding method is applied to binarize the image (c), and additional processing is undertaken to remove the extraneous parts of the image by identifying the largest particle and the one that has roundness between 0.1 and 1.0 (d).

using the method of Thévenaz et al. (1998) which seeks to minimise the mean square intensity difference between images by rotation and translation, thus using all the features of the outline of the operculum. The resulting registration values can be used to rotate and translate the visible images, and animation of these transformed visible images provides a rapid method for the analyst to qualitatively assess the success of the registration process (Supplementary Information S1). This visual record shows the extent to which the operculum moves, but also shows that the steel cups in which the sample is mounted tend to rotate, and are also subject to small lateral movements.

Rotating the visible images is suitable for providing a qualitative assessment of the success of the registration process, but this approach is not applied to the images of the luminescence signal. Instead a coordinate system is defined for each image, based on the orientation of the operculum. The translation and rotation determined by the method of Thévenaz et al. (1998) is then applied to the coordinate system to mirror the movement of the operculum (Fig. 3). The result is that a region of interest (ROI) that is defined in the coordinate system remains fixed relative to the object of interest. This is based on the approach that was previously adopted for single grains in the Viewer + software (as outlined in Kook et al., 2015), but in that case the orientation of the sample disc was determined by tracking the three locating holes around the periphery of the single grain discs used. Adopting this same approach here makes it possible to use the Viewer + software to perform the signal integration, whilst accounting for movement of the sample on the disc, as well as movement of the sample holder itself.

5. Implementation of tracking and registration algorithms

Data collected using the EMCCD system implemented by Kook et al. (2015) consists of a complex pattern of files, consisting of multiple-frame TIFF files for the luminescence data, a separate single-frame TIFF file of the reflected light image of the sample collected after measurement of the luminescence, and a single BINX file that contains data about the measurement conditions, but no luminescence data. To implement the approach described here involves a series of operations in ImageJ, manipulation of the results from tracking, and then creation of data that allows a coordinate system to be defined for each aliquot, and regions of interest defined across the surface of the object. An ImageJ macro has been written in the FIJI environment to automate the first 7 steps of this process (Fig. 4) (Duller and Roberts, 2024). The data for defining the coordinate system, and the definitions of the regions of interest are then transferred to the BINX file within a specially modified version of the Analyst programme (Duller 2015). Viewer+ is then used to integrate the luminescence data in the regions of interest to generate TL glow curves for each ROI in the BINX file. Within Viewer + we also use a routine based on the use of a median filter to remove the impact of hotspots on our extracted TL data. The BINX file can then be analysed using Analyst, with each ROI appearing as a "single grain". The raw luminescence images collected by the EMCCD are also available within Analyst, and the position of each ROI within that image is shown.

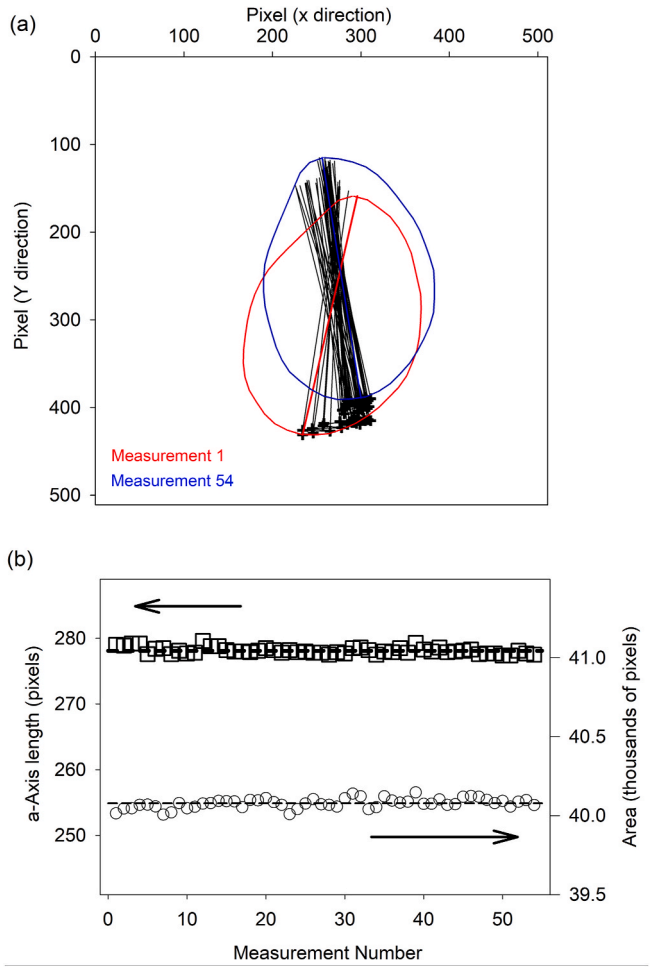

Fig. 2. (a) Movement of one operculum during a sequence of 54 measurements. Each pixel images an area 19 by 19 μm on the sample. The black lines show the position of the a-axis of the operculum. The outline of the operculum identified by the thresholding method is shown for measurement 1 (in red) and measurement 54 (in blue). (b) In spite of the movement of the operculum, the measured length of the a-axis and the area of the operculum remain consistent across all 54 measurements. (For interpretation of the references to color in this figure legend, the reader is referred to the Web version of this article).

6. Application of the registration process for dose recovery

To assess the accuracy of the tracking and registration process described above, a dose recovery experiment was undertaken. An operculum that had previously been heated to 400 °C and had any natural TL signal removed was given a dose of 405 Gy, and the SAR sequence shown in Table 1 applied to attempt to recover this dose. A set of 8 regeneration doses, including two measurements of the response to zero and 324 Gy was undertaken.

The data set was first interrogated by summing the emission from a single circular region of interest that covered the entire sample cup, and thus was not affected by movement of the operculum. This yielded a single value for the dose recovery ratio of 1.02 ± 0.03. Spatially-resolved data analysis was then undertaken by defining a grid of regions of interest (ROIs) across the surface of the operculum. ROIs were chosen to be 15 pixels by 15 pixels (approximately 285 by 285 μm) in size. The choice of ROI size is arbitrary and other values could be used, but as smaller ROIs are used signal intensity decreases, and this can lead to more noisy data. Additionally, since luminescence may be emitted in all directions from both the surface and the interior of the operculum, some spatial averaging of the emitted signal occurs, and so there is little point using an ROI that is much smaller than that used here. The regular

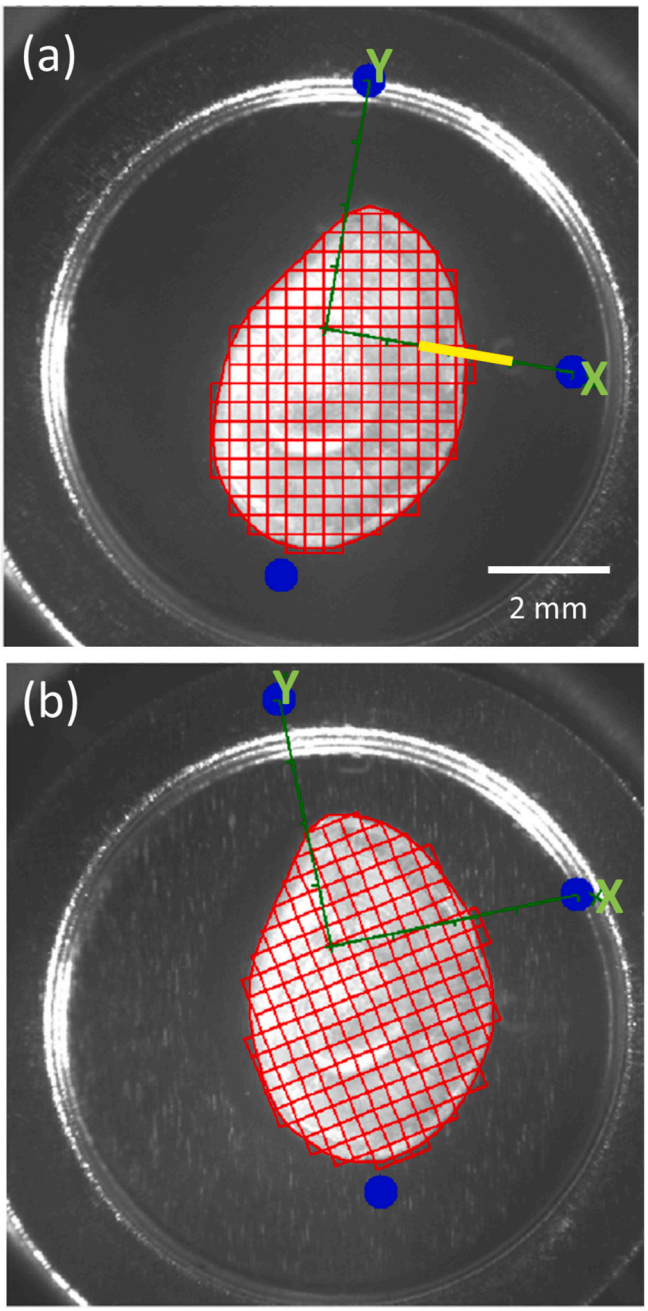

Fig. 3. The first (a) and last (b) image collected for the operculum shown in Fig. 2. The coordinate system defined for each image is shown and can be seen to be translated and rotated with the operculum. The blue dots three artificial markers that are used for processing and do not represent any physical markers. A set of regions of interest (15 by 15 pixels in size) are also shown in red, define within the coordinate system. The yellow bar shown in (a) is the position of the 1500 μm long transect shown in Fig. 6. In order to make the transect visible on this figure, the thickness of the transect is approximately double its actual thickness (~57 μm).

grid of ROIs was restricted to the outline of the operculum defined by the threshold step described in Section 3. ROIs were defined where the four vertices all fell within the outline of the operculum. At the margins an ROI was included where three of its four vertices fell within the operculum, but if two or more vertices are outside the operculum it was not included. Using this procedure 177 ROIs were defined across the surface of the operculum.

Two analyses of the data were undertaken to determine equivalent

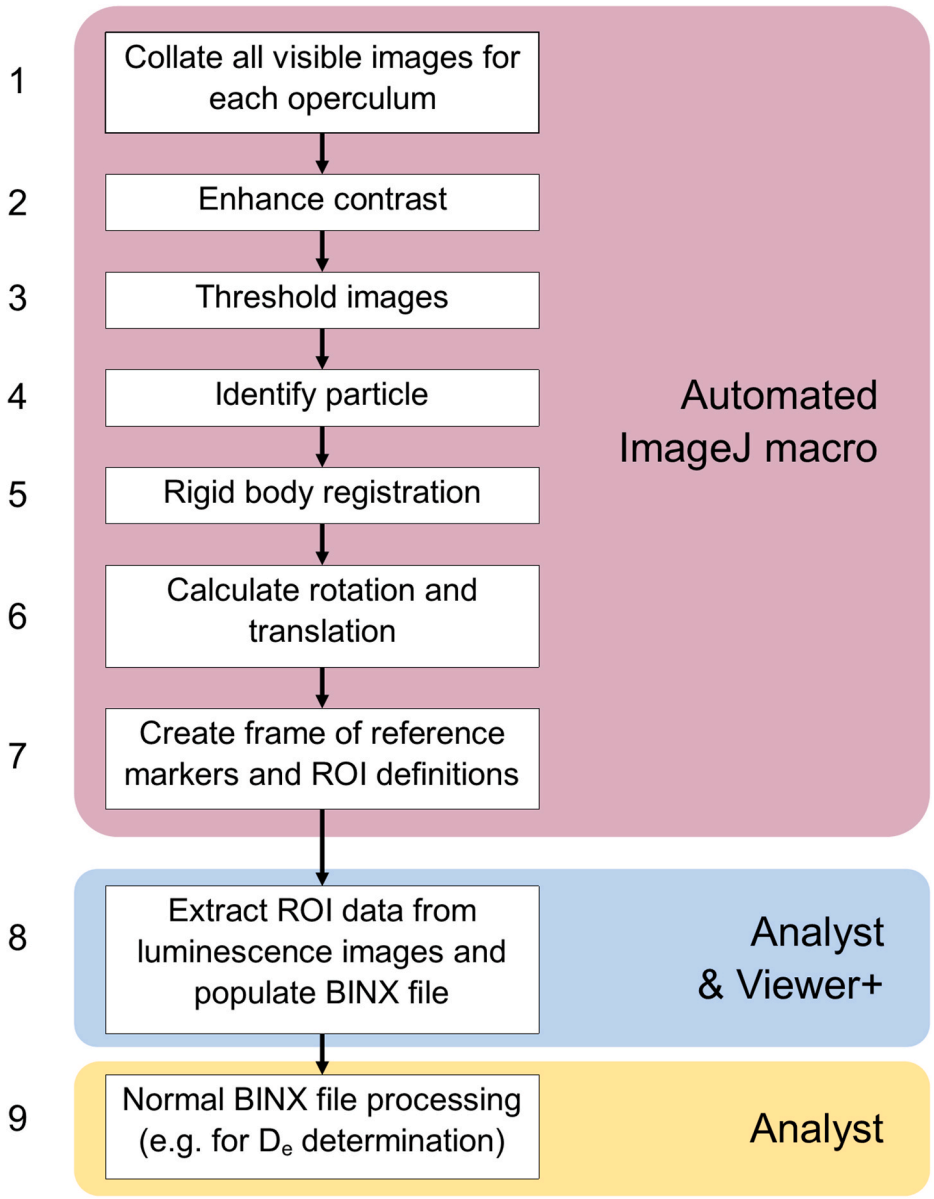

Fig. 4. Flow chart of the operations required to process opercula luminescence data. The parts of the process automated in ImageJ, and those requiring Analyst and Viewer + are shown.

dose values, and hence calculate the spatially-resolved dose recovery ratio. The first was designed to illustrate what happens if no allowance is made for movement of the operculum. In this case the position of the ROIs was defined in terms of the 512 by 512 image array, and no correction was applied to allow for movement of the operculum within the image. The second analysis used the tracking and registration procedure to define a coordinate system, and the coordinate system was moved relative to the position of the operculum. The ROIs were defined within this coordinate system, and hence moved with the operculum.

It is no surprise that in the first analysis, the outcome of failing to correct for movement of the operculum is that many of the ROIs yield dose response curves that appear very noisy, that 85 out of 177 of the ROIs yield recycling ratios outside the range of 0.9–1.1 (no account has been taken here of the uncertainty on the recycling ratios), and that even where the recycling ratio does fall within the range 0.9–1.1 the values of the dose recovery ratio vary from 0.7 to more than 1.2 (Fig. 5a). However, when the procedure described in Sections 3 and 4 is applied to define the ROIs in terms of a coordinate system that moves with the operculum, 172 out of 177 ROIs yield recycling ratios within the range 0.9–1.1, the values of dose recovery are consistent with unity within two sigma, show little scatter (Fig. 5b), and have an overdispersion value of 0.0 %. The mean of the dose recovery ratio data for the 172 ROIs that passed the recycling criterion is 1.00 ± 0.02 (uncertainty expressed as a standard deviation of the 172 ROI values).

To further illustrate the impact of the registration process upon the TL data, a profile of the TL signal intensity across the edge of the operculum was calculated for each preheat of the test dose. The preheat of the test dose was selected because the low temperature (~100 °C) TL peak provides an intense signal, and shows limited sensitivity change. The transect was 1500 μm in length, and was 3 pixels wide (~57 μm). Prior to registration the transect is defined in relation to the camera and the edge of the operculum is seen to move relative to this coordinate system (Fig. 6a), but when the transect is defined in terms of the coordinate system derived from application of the registration procedure outlined in Fig. 4, the edge of the operculum remains at a constant position (Fig. 6b).

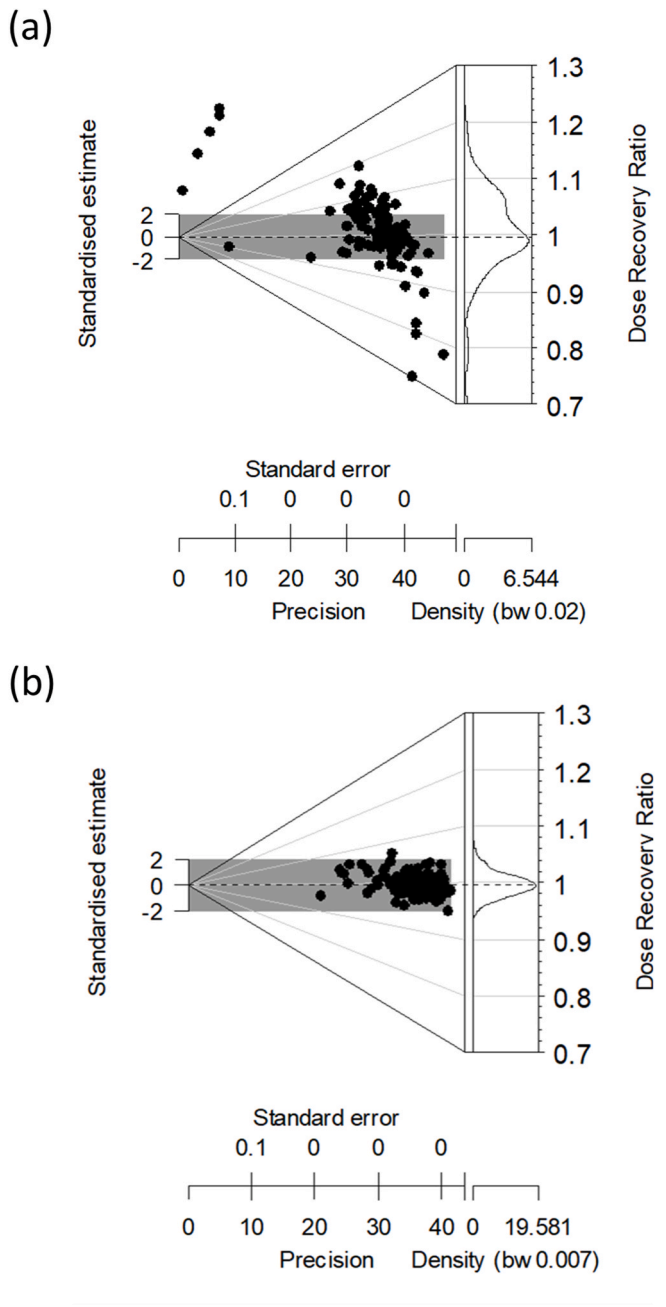

Fig. 5. Abanico plots showing the result of a dose recovery experiment for an operculum given 405 Gy. A grid of 177 regions of interest (each 15 by 15 pixels in size) were used for analysis. (a) When the position of the ROIs is not corrected for movement of the operculum a wide range of dose recovery ratios is seen. (b) When the tracking and registration process described in the paper are applied and used to define a coordinate system for the ROIs, the values of dose recovery ratio are consistent with unity and within the two sigma band.

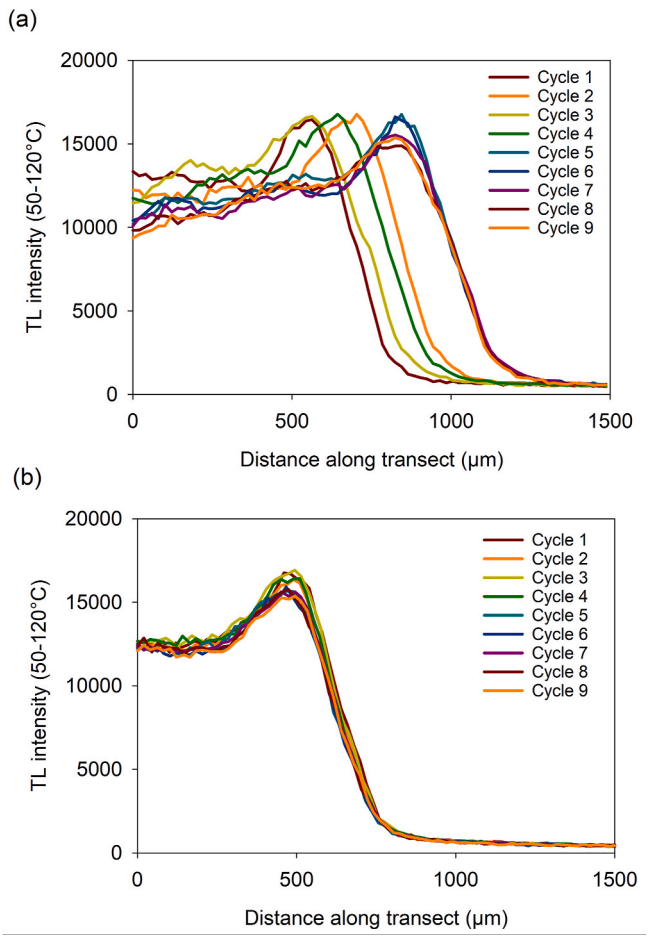

Fig. 6. TL signal intensity across the edge of the operculum for each of the 9 cycles of the SAR sequence. The position of the transect is shown by the yellow bar on Fig. 3a. The TL signal resulting from preheating the test dose is summed from 50 to 120 °C for a transect 3 pixels wide (~57 μm) and 1500 μm long. (a) Transects obtained prior to any registration of the TL data, and (b) after application of the registration process described in Fig. 4.

7. Discussion

Opercula placed on steel cups undergo movement between measurement steps, and the steel cups upon which they sit also rotate and undergo some limited lateral movement. Correcting for this movement is crucial prior to the analysis of signal intensity of regions of interest to ensure that the TL emission is consistently being observed from the same part of the sample. The process outlined here provides a reproducible and rapid method of registration and has been implemented using the ImageJ Macro language to automate the process. The method outlined here moves the regions of interest to ensure that they follow the movement of the sample. An alternative approach could be envisaged where the luminescence images collected are rotated and translated. This approach would make subsequent analysis simpler, but rotation of images without altering the intensity is extremely difficult, and makes that approach less viable. Once the regions of interest have been defined by the ImageJ macro and added to the BINX file, Viewer+ is used to then sum the signal from the regions of each luminescence image file to create a BINX file containing TL glow curves for each ROI. Further streamlining of the workflow could be achieved in the future by using ImageJ to perform this summing, though it would likely be significantly slower than Viewer+.

The method described here has been designed specifically for analysis of opercula, but the same principle could be extended to look at other solid samples, such as slug plates (Duller et al., 2009), and rock slices, though it should be noted that the procedure described here is not applicable to perfectly circular objects as any rotation would not be detected. Modification of the rock slices by cutting notches into them, working with non-circular slices or some similar approach, would be needed to allow this procedure to work. The approach could also be adapted to enable registration of images captured by different cameras mounted on the same instrument, such as the imaging infrared photoluminescence (IRPL) detector SIRIOL (Gunn et al., 2022).

As well as allowing automated registration of images, numerical processing of the images also allows automated quantification of other parameters such as object surface area, the a- and b-axis length, and the

degree of circularity to be calculated, and these parameters would be of value for dosimetry calculations of such objects.

8. Conclusions

The results shown here demonstrate that the method outlined in Fig. 4 provides an accurate and objective method for registering images of opercula, enabling the establishment of a coordinate system that tracks the object being measured. By defining regions of interest in relation to this coordinate system, the ROIs track the object even if it moves or rotates during a sequence of measurements. The registration of images is essential for spatially resolved analysis of these opercula, including calculating spatially resolved equivalent dose determination. The approach could also be extended to a range of other samples that could be analysed using imaging luminescence detectors.

CRediT authorship contribution statement

G.A.T. Duller: Conceptualization, Formal analysis, Funding acquisition, Software, Writing – original draft, Writing – review & editing. **H. M. Roberts:** Conceptualization, Funding acquisition, Writing – review & editing.

Declaration of competing interest

The authors declare that they have no known competing financial interests or personal relationships that could have appeared to influence the work reported in this paper.

Data availability

The ImageJ script used in this work is contained in Supplementary Information along with an example set of images

Acknowledgements

This work arises from a project that has received funding from the European Research Council (ERC) under the European Union's Horizon 2020 research and innovation programme (grant –agreement No. 865222; 'EQuaTe' –'Bridging Europe: A Quaternary Timescale for the Expansion and Evolution of Humans'). Capital funding for the EMCCD was from the Higher Education Funding Council for Wales (HEFCW) to support the creation of the SPARCL (SPAtially Resolved geoChronoLogy) facility in the Department of Geography and Earth Sciences at Aberystwyth University. Our thanks to Anna Maartje de Boer, Jakob Wallinga and an anonymous referee for their comments which helped to improve the clarity of the manuscript.

Appendix A. Supplementary data

Supplementary data to this article can be found online at https://doi.org/10.1016/j.radmeas.2024.107084 and the ImageJ script can be found at Roberts (2024).

References

Bailiff, I.K., Mikhailik, V.B., 2003. Spatially-resolved measurement of optically stimulated luminescence and time-resolved luminescence. Radiat. Meas. 37, 151–159.
Baril, M.R., 2004. CCD imaging of the infra-red stimulated luminescence of feldspars. Radiat. Meas. 38, 81–86.
Bøtter-Jensen, L., Bulur, E., Duller, G.A.T., Murray, A.S., 2000. Advances in luminescence instrument systems. Radiat. Meas. 32, 523–528.
Clark-Balzan, L., Schwenninger, J.-L., 2012. First steps toward spatially resolved OSL dating with electron multiplying charge-coupled devices (EMCCDs): system design and image analysis. Radiat. Meas. 47, 797–802.
Duller, G.A.T., 2015. The Analyst software package for luminescence data: overview and recent improvements. Ancient TL 33, 35–42.
Duller, G.A.T., Bøtter-Jensen, L., Markey, B.G., 1997. A luminescence imaging system based on a charge coupled device (CCD) camera. Radiat. Meas. 27, 91–99.
Duller, G.A.T., Bøtter-Jensen, L., Kohsiek, P., Murray, A.S., 1999. A high-sensitivity optically stimulated luminescence scanning system for measurement of single sand-sized grains. Radiat. Protect. Dosim. 84, 325–330.
Duller, G.A.T., Kook, M., Stirling, R.J., Roberts, H.M., Murray, A.S., 2015. Spatially-resolved thermoluminescence from snail opercula using an EMCCD. Radiat. Meas. 81, 157–162.
Duller, G.A.T., Roberts, H.M., 2018. Seeing snails in a new light: luminescence dating using calcite. Elements 14, 39–43.
Duller, G.A.T., Penkman, K.E.H., Wintle, A.G., 2009. Assessing the potential for using biogenic calcites as dosemeters for luminescence dating. Radiat. Meas. 44, 429–433.
Duller, G.A.T., Roberts, H.M., 2024. Chasing snails: automating the processing of EMCCD images of luminescence from opercula. Mendeley Data V1. https://doi.org/10.17632/5t9f6kjh2x.1.
Greilich, S., Glasmacher, U.A., Wagner, G.A., 2002. Spatially resolved detection of luminescence: a unique tool for archaeochronometry. Naturwissenschaften 89, 371–375.
Gunn, M., Duller, G.A.T., Roberts, H.M., 2022. SIRIOL: a sensitive InfraRed instrument for phOto luminescence measurements of feldspar. Radiat. Meas. 154, 106782.
Hashimoto, T., Kimura, K., Koyangi, A., Takahashi, K., Sotobayashi, T., 1983. New colour-photographic observation of thermoluminescence from sliced rock samples. Radioisotopes 32, 525–532.
Kook, M., Lapp, T., Murray, A.S., Thomsen, K.J., Jain, M., 2015. A luminescence imaging system for the routine measurement of single-grain OSL dose distributions. Radiat. Meas. 81, 171–177.
McWhirter, I., 2008. Electron Multiplying CCDs – new technology for low light level imaging. IRF Sci. Rep. 292, 61–66.
Richter, D., Richter, A., Dornich, K., 2013. Lexsyg – a new system for luminescence research. Geochronometria 40, 220–228.
Sanderson, D.C.W., Carmichael, L., Murphy, S., Whitely, V., Scott, E., Cresswell, A., 2001. Investigation of Statistical and Imaging Methods for Luminescence Detection of Irradiated Ingredients. In: Project Report CSA, vol. 5240. Food Standards Agency, London, UK.
Schneider, C.A., Rasband, W.S., Eliceiri, K.W., 2012. NIH Image to ImageJ: 25 years of image analysis. Nat. Methods 9, 671–675.
Sellwood, E.L., Kook, M., Jain, M., 2022. A 2D imaging system for mapping luminescence-depth profiles for rock surface dating. Radiat. Meas. 150, 106697.
Sezgin, M., Sankur, B., 2004. Survey over image thresholding techniques and quantitative performance evaluation. J. Electron. Imag. 13 (1), 146–168.
Smith, B.W., Wheeler, G.C.W.S., Rhodes, E.J., Spooner, N.A., 1991. Luminescence dating of zircon using an imaging photon detector. Nucl. Tracks Radiat. Meas. 18, 273–278.
Thévenaz, P., Ruttimann, U.E., Unser, M., 1998. A pyramid approach to subpixel registration based on intensity. IEEE Trans. Image Process. 7 (1), 27–41.
Walton, A.J., Debenham, N.C., 1980. Spatial-distribution studies of thermoluminescence using a high-gain image intensifier. Nature 284, 42–44.